

NJC

Accepted Manuscript



This article can be cited before page numbers have been issued, to do this please use: D. Chen, L. Lin, T. Sheng, Y. Wen, X. Zhu, L. Zhang, S. Hu, R. Fu and X. Wu, *New J. Chem.*, 2018, DOI: 10.1039/C7NJ04048B.



This is an Accepted Manuscript, which has been through the Royal Society of Chemistry peer review process and has been accepted for publication.

Accepted Manuscripts are published online shortly after acceptance, before technical editing, formatting and proof reading. Using this free service, authors can make their results available to the community, in citable form, before we publish the edited article. We will replace this Accepted Manuscript with the edited and formatted Advance Article as soon as it is available.

You can find more information about Accepted Manuscripts in the [author guidelines](#).

Please note that technical editing may introduce minor changes to the text and/or graphics, which may alter content. The journal's standard [Terms & Conditions](#) and the ethical guidelines, outlined in our [author and reviewer resource centre](#), still apply. In no event shall the Royal Society of Chemistry be held responsible for any errors or omissions in this Accepted Manuscript or any consequences arising from the use of any information it contains.



Journal Name

ARTICLE

Syntheses, structures, luminescence and magnetic properties of seven isomorphous metal-organic frameworks based on 2,7-bis(4-benzoic acid)-N-(4-benzoic acid) carbazole

Dong-Hui Chen^{ab}, Ling Lin^{ab}, Tian-Lu Sheng^a, Yue-Hong Wen^a, Xiao-Quan Zhu^{ab}, Lin-Tao Zhang^{ab}, Sheng-Min Hu^a, Rui-Biao Fu^a and Xin-Tao Wu^{*a}

Received 00th January 20xx,
Accepted 00th January 20xx

DOI: 10.1039/x0xx00000x

www.rsc.org/

We report herein seven novel lanthanide metal-organic frameworks (Ln-MOFs), $[M(L_{27})(DMA)(H_2O) \cdot xH_2O]_n$ (**TCZ-M**), (**M** = Nd, Sm, Eu, Gd, Tb, Dy, Ho), (**X** = 2 or 3) (**H₃L₂₇** = 2,7-bis(4-benzoic acid)-N-(4-benzoic acid) carbazole, DMA = N,N-dimethylacetamide, TCZ = "T"-shape carbazole-based MOFs, **L₂₇** = fully deprotonated **H₃L₂₇³⁻** ligand). X-ray crystallography showed that all of the **TCZ-M** (**M** = Nd, Sm, Eu, Gd, Tb, Dy, Ho) are isomorphous and possesses a 3,6-connected three-dimensional (3D) framework with a point symbol of $\{4-6^2\}_2\{4^2-6^{10}-8^3\}$. The photoluminescence measurement indicates that **TCZ-Eu** shows reddish-orange emission bands and **TCZ-Sm** shows both visible and near-infrared (NIR) emissions bands. Magnetic susceptibility measurements show deviations from the Curie law mainly owing to the split of the ground term due to the ligand field and spin-orbit coupling in **TCZ-Eu** and **TCZ-Sm**. The magnetic properties of **TCZ-M** (**M** = Nd, Gd, Tb, Dy, Ho) are also investigated, and the results indicate a ferromagnetic interaction between Tb³⁺ magnetic centers in TCZ-Tb and antiferromagnetic interactions in **TCZ-M** (**M** = Nd, Gd, Dy, Ho).

Introduction

Metal-organic frameworks (MOFs), assembled from organic linkers and metal nodes, have been explored for potential application in optical, magnetic, separation, gas sorption and catalysis fields.¹ The flexibility of organic linkers and metal nodes provides the opportunity for engineering the properties and structures of the MOFs.²

The research on lanthanide metal-organic frameworks (Ln-MOFs), usually composed of trivalent lanthanide ions and aromatic multicarboxylate ligands, is an important branch of the study in MOFs fields.³ Trivalent lanthanide ions have attracted great attention due to their intense and sharp f→f emissions. For example, Eu³⁺ ion and Sm³⁺ ion have rich spectroscopic properties as a result of multifold electronic transitions. The Ln-MOFs based on Eu³⁺ ions usually emit red luminescence due to the multifold electronic transitions originating from the ⁵D₀ energy level to ⁷F_J and the Ln-MOFs based on Sm³⁺ ions emit visible and near-infrared (NIR) emissions sometimes which due to the multifold electronic

transitions originating from the ⁴G_{5/2} energy level to ⁶H_J (visible) and ⁶F_J (NIR). The properties of Ln-MOFs could be used in potential applications in light-emitting diodes (LEDs), biological applications (such as immunoassay and magnetic resonance imaging), photoluminescent sensors.⁴ Unique magnetic properties are also one of the advantages of trivalent lanthanide ions.⁵ Thus, Ln-MOFs based on trivalent lanthanide ions are ideal multifunctional materials, as they are able to incorporate with the porous properties, magnetic properties and photoluminescent properties.⁶ However, the forbidden f-f transitions of lanthanide ions exhibit a very small molar absorption coefficient and relatively weak UV absorption with low luminous efficiency.⁷ Fortunately, the aromatic multicarboxylate compound is one of the most important organic ligands in construction of functionalized metal-organic frameworks.⁸ And it was often used as bridge ligands for construction of luminescent Ln-MOFs. Because it has strong absorption (conjugate with rigid structures) in the ultraviolet region which is called "antenna effect".⁹ The lanthanide metal-organic frameworks, assembled with aromatic multicarboxylate ligands, may perform excellent "antenna effect".¹⁰ Therefore, with excellent structural diversity and amazing physical properties related to unique 4f-electrons, Ln-MOFs occupy a special position among MOFs. Recently, there are some works about Ln-MOFs has been reported already according to these phenomena.¹¹

Considering all of the above-mentioned, 2,7-bis(4-benzoic acid)-N-(4-benzoic acid) carbazole (**H₃L₂₇**), a conjugated tricarboxylic acid ligand, was employed as an organic linker. And its reaction with the nitrates of trivalent lanthanide ions

^a State Key Laboratory of Structure Chemistry, Fujian Institute of Research on the Structure of Matter, Chinese Academy of Sciences, Fuzhou 350002, Fujian, PR China.

E-mail: wxl@fjirsm.ac.cn

^b University of the Chinese Academy of Sciences, Beijing, 100049, China.

Electronic Supplementary Information (ESI) available: Selected bond lengths and angles, PXRD curve, TGA curve, IR spectra, UV-Vis spectra. CCDC-1553995 for TCZ-Nd, CCDC-1553996 for TCZ-Sm, CCDC-1553997 for TCZ-Eu, CCDC-1553998 for TCZ-Gd, CCDC-1553999 for TCZ-Tb, CCDC-1554000 for TCZ-Dy, CCDC-1554001 for TCZ-Ho. For ESI and crystallographic data in CIF or other electronic format see DOI: 10.1039/x0xx00000x.

was predicted to form novel functional Ln-MOFs. Herein, we present seven three-dimensional Ln-MOFs, $[\text{M}(\text{L}_{27})(\text{DMA})(\text{H}_2\text{O})\cdot\text{XH}_2\text{O}]_n$ (**TCZ-M**), (**M** = Nd, Sm, Eu, Gd, Tb, Dy, Ho), (**X** = 2 or 3) (DMA = N,N-dimethylacetamide, TCZ = "T"-shape carbazole-based MOFs), which exhibit good luminescent and magnetic properties, respectively.

Experimental

Materials and Methods

Potassium tert-butoxide, 4,4'-dibromobiphenyl, ethyl 4-fluorobenzoate, potassium carbonate, tetrakis(triphenylphosphine)palladium(0), $\text{Nd}(\text{NO}_3)_3\cdot 6\text{H}_2\text{O}$, $\text{Sm}(\text{NO}_3)_3\cdot 6\text{H}_2\text{O}$, $\text{Eu}(\text{NO}_3)_3\cdot 6\text{H}_2\text{O}$, $\text{Gd}(\text{NO}_3)_3\cdot 6\text{H}_2\text{O}$, $\text{Tb}(\text{NO}_3)_3\cdot 6\text{H}_2\text{O}$, $\text{Dy}(\text{NO}_3)_3\cdot 6\text{H}_2\text{O}$, $\text{Ho}(\text{NO}_3)_3\cdot 6\text{H}_2\text{O}$ and solvents were purchased commercially and used directly. Elemental analyses (C, H and N) were performed with an Elementar Vario EL-Cube Element Analyzer. Powder X-ray diffraction (PXRD) data were collected on a Rigaku MiniFlex 600 diffractometer using $\text{Cu K}\alpha$ radiation ($\lambda = 0.154 \text{ nm}$). Infrared spectra were recorded with KBr pellets in the range $4000\text{--}400\text{cm}^{-1}$ on a Perkin-Elmer Spectrum One FT-IR spectrometer. Thermogravimetric analysis (TGA) experiments were carried out on a NETZSCH STA 449C Jupiter thermogravimetric analyzer in flowing nitrogen with the sample heated in an Al_2O_3 crucible from room temperature to $1000 \text{ }^\circ\text{C}$ at a heating rate of $10 \text{ K}\cdot\text{min}^{-1}$. Metal elemental analyses (for lanthanide metal ions) were performed with a

HORIBA Jobin Yvon Ultima2 Inductively Coupled Plasma OES spectrometer (ICP). Magnetic susceptibilities of crystalline samples were measured with a Quantum Design MPMS-XL SQUID susceptometer under an applied magnetic field of 1 kOe in the $2\text{--}300 \text{ K}$ range. Diamagnetic corrections were made using Pascal's constants.¹²

Synthesize of 2,7-bis(4-benzoic acid)-N-(4-benzoic acid) carbazole (**H₃L₂₇**):

The synthesis in this work start from commercially available 4,4'-dibromobiphenyl. **H₃L₂₇** was synthesized according to the literature procedure and the synthetic method is shown in Supporting Information. (Scheme S1)¹³

Synthesis of $[\text{Nd}(\text{L}_{27})(\text{DMA})(\text{H}_2\text{O})\cdot 3\text{H}_2\text{O}]_n$ (**TCZ-Nd**)

Solvothermal reaction of $\text{Nd}(\text{NO}_3)_3\cdot 6\text{H}_2\text{O}$ (21.9 mg, 0.05 mmol), 2,7-bis(4-benzoic acid)-N-(4-benzoic acid) carbazole (**H₃L₂₇**) (26.3 mg, 0.05 mmol) in the mixture of N,N'-dimethylacetamine (DMA) (2 ml) and H_2O (0.5 ml) at 348 K for 4 days gave rise to lavender prism crystals of **TCZ-Nd** (19.3 mg, Yield: 48.8%). Anal. Calcd (%) for $\text{C}_{37}\text{H}_{35}\text{N}_2\text{O}_{11}\text{Nd}$: C 53.67, H 4.26, N 3.38. Found: C 53.66, H 4.26, N 3.38.

Synthesis of $[\text{Sm}(\text{L}_{27})(\text{DMA})(\text{H}_2\text{O})\cdot 3\text{H}_2\text{O}]_n$ (**TCZ-Sm**)

Solvothermal reaction of $\text{Sm}(\text{NO}_3)_3\cdot 6\text{H}_2\text{O}$ (22.2 mg, 0.05 mmol), 2,7-bis(4-benzoic acid)-N-(4-benzoic acid) carbazole (**H₃L₂₇**) (26.3 mg, 0.05 mmol) and 69% concentrated nitric acid ($10 \mu\text{L}$),

Table 1 Crystal and X-ray experimental data for compounds **TCZ-Nd**, **TCZ-Sm**, **TCZ-Eu**, **TCZ-Gd**

Compound	TCZ-Nd	TCZ-Sm	TCZ-Eu	TCZ-Gd
Empirical formula	$\text{C}_{37}\text{H}_{35}\text{N}_2\text{O}_{11}\text{Nd}$	$\text{C}_{37}\text{H}_{33}\text{N}_2\text{O}_{10}\text{Sm}$	$\text{C}_{37}\text{H}_{33}\text{N}_2\text{O}_{10}\text{Eu}$	$\text{C}_{37}\text{H}_{33}\text{N}_2\text{O}_{10}\text{Gd}$
Formula weight	827.91	816.00	817.60	822.90
Crystal system	Monoclinic	Monoclinic	Monoclinic	Monoclinic
Space group	$P2_1/c$	$P2_1/c$	$P2_1/c$	$P2_1/c$
<i>a</i> (Å)	15.986(7)	15.793(7)	15.776(3)	15.696(4)
<i>b</i> (Å)	8.403(3)	8.363(3)	8.3587(16)	8.307(2)
<i>c</i> (Å)	28.487(13)	28.515(12)	28.529(5)	28.470(8)
α (°)	90	90	90	90
β (°)	96.253(5)	96.516(7)	96.501(4)	96.418(5)
γ (°)	90	90	90	90
<i>V</i> (Å ³)	3804(3)	3742(3)	3737.9(12)	3689.0(17)
<i>Z</i>	4	4	4	4
Temperature(K)	293(2)	293(2)	293(2)	293(2)
<i>D</i> (Mg m ⁻³)	1.445	1.448	1.453	1.517
μ (mm ⁻¹)	1.414	1.619	1.727	1.848
<i>F</i> (000)	1676	1644	1648	1652
$R_1^a, wR2_b(I > 2\sigma(I))$	0.0879, 0.1979	0.0770, 0.1846	0.0530, 0.1253	0.0496, 0.1199
θ_{ranges} (deg)	2.53 to 27.51	2.59 to 27.46	2.54 to 27.52	2.55 to 27.49
<i>h, k, l</i> ranges	$-20 \leq h \leq 20$	$-20 \leq h \leq 20$	$-20 \leq h \leq 20$	$-17 \leq h \leq 20$
	$-10 \leq k \leq 8$	$-10 \leq k \leq 10$	$-10 \leq k \leq 10$	$-10 \leq k \leq 10$
	$-36 \leq l \leq 36$	$-36 \leq l \leq 33$	$-36 \leq l \leq 35$	$-36 \leq l \leq 36$
GOF on F^2	1.169	1.125	1.108	1.133

$$^a R = \sum |F_o| - F_c / \sum |F_o|, \quad ^b wR_2 = [P[w(F_o^2 - F_c^2)^2] / \sum [(F_o^2)^2]]^{1/2}$$

Table 2 Crystal and X-ray experimental data for compounds **TCZ-Tb**, **TCZ-Dy**, **TCZ-Ho**.

Compound	TCZ-Tb	TCZ-Dy	TCZ-Ho
Empirical formula	C ₃₇ H ₃₃ N ₂ O ₁₀ Tb	C ₃₇ H ₃₃ N ₂ O ₁₀ Dy	C ₃₇ H ₃₃ N ₂ O ₁₁ Ho
Formula weight	824.57	828.15	848.60
Crystal system	Monoclinic	Monoclinic	Monoclinic
Space group	<i>P</i> 2 ₁ / <i>c</i>	<i>P</i> 2 ₁ / <i>c</i>	<i>P</i> 2 ₁ / <i>c</i>
<i>a</i> (Å)	15.729(4)	15.735(7)	15.682(5)
<i>b</i> (Å)	8.3089(18)	8.290(3)	8.316(3)
<i>c</i> (Å)	28.483(7)	28.436(12)	28.526(11)
α (°)	90	90	90
β (°)	96.448(4)	96.414(8)	96.325(9)
γ (°)	90	90	90
<i>V</i> (Å ³)	3699.1(14)	3686(3)	3697(2)
<i>Z</i>	4	4	4
Temperature(K)	293(2)	293(2)	293(2)
<i>D</i> (Mg m ⁻³)	1.481	1.492	1.524
μ (mm ⁻¹)	1.962	2.077	2.19
<i>F</i> (000)	1656	1660	1704
<i>R</i> ₁ ^a , <i>wR</i> ₂ b(1>2 σ (<i>I</i>))	0.0573, 0.1373	0.0511, 0.1250	0.0842, 0.1685
θ _{ranges} (deg)	2.55 to 27.51	2.56 to 27.47	2.55 to 27.50
<i>h, k, l</i> ranges	-20 ≤ <i>h</i> ≤ 20 -10 ≤ <i>k</i> ≤ 10 -35 ≤ <i>l</i> ≤ 36	-20 ≤ <i>h</i> ≤ 20 -10 ≤ <i>k</i> ≤ 10 -36 ≤ <i>l</i> ≤ 36	-17 ≤ <i>h</i> ≤ 20 -10 ≤ <i>k</i> ≤ 10 -36 ≤ <i>l</i> ≤ 36
GOF on <i>F</i> ²	1.119	1.094	1.183

$$^a R = \sum |F_o| - F_c| / \sum |F_o|, \quad ^b wR_2 = [P[w(F_o^2 - F_c^2)^2] / \sum [(F_o^2)^2]]^{1/2}$$

which is used for regulating the *pH* value, in the mixture of DMA (2 ml) and H₂O (0.5 ml) at 348 K for 4 days gave rise to lavender prism crystals of **TCZ-Sm** (17.8 mg, Yield: 44.9%). Anal. Calcd (%) for C₃₇H₃₅N₂O₁₁Sm: C 53.28, H 4.23, N 3.36. Found: C 53.28, H 4.25, N 3.35.

Synthesis of [Eu(L₂₇)(DMA)(H₂O)·2H₂O]_n (TCZ-Eu)

Solvothermal reaction of Eu(NO₃)₃·6H₂O (22.3 mg, 0.05 mmol), 2,7-bis(4-benzoic acid)-N-(4-benzoic acid) carbazole (**H₃L₂₇**) (26.3 mg, 0.05 mmol) and 69% concentrated nitric acid (10 μL) in the mixture of DMA (2 ml) and H₂O (0.5 ml) at 348 K for 4 days gave rise to lavender prism crystals of **TCZ-Eu** (24.3 mg, Yield: 60.9%). Anal. Calcd (%) for C₃₇H₃₃N₂O₁₀Eu: C 54.35, H 4.07, N 3.42. Found: C 54.36, H 4.06, N 3.41.

Synthesis of [Gd(L₂₇)(DMA)(H₂O)·2H₂O]_n (TCZ-Gd)

Solvothermal reaction of Gd(NO₃)₃·6H₂O (22.5 mg, 0.05 mmol), 2,7-bis(4-benzoic acid)-N-(4-benzoic acid) carbazole (**H₃L₂₇**) (26.3 mg, 0.05 mmol) and 69% concentrated nitric acid (20 μL) in the mixture of DMA (2 ml) and H₂O (0.5 ml) at 348 K for 4 days gave rise to lavender prism crystals of **TCZ-Gd** (20.6 mg,

Yield: 51.0%). Anal. Calcd (%) for C₃₇H₃₃N₂O₁₀Gd: C 54.00, H 4.04, N 3.40. Found: C 54.06, H 4.05, N 3.39.

Synthesis of [Tb(L₂₇)(DMA)(H₂O)·2H₂O]_n (TCZ-Tb)

Solvothermal reaction of Tb(NO₃)₃·6H₂O (22.6 mg, 0.05 mmol), 2,7-bis(4-benzoic acid)-N-(4-benzoic acid) carbazole (**H₃L₂₇**) (26.3 mg, 0.05 mmol) and 69% concentrated nitric acid (20 μL) in the mixture of DMA (2 ml) and H₂O (0.5 ml) at 348 K for 4 days gave rise to lavender prism crystals of **TCZ-Tb** (20.4 mg, Yield: 50.6%). Anal. Calcd (%) for C₃₇H₃₃N₂O₁₀Tb: C 53.89, H 4.03, N 3.40. Found: C 53.90, H 4.02, N 3.40.

Synthesis of [Dy(L₂₇)(DMA)(H₂O)·2H₂O]_n (TCZ-Dy)

Solvothermal reaction of Dy(NO₃)₃·6H₂O (22.8 mg, 0.05 mmol), 2,7-bis(4-benzoic acid)-N-(4-benzoic acid) carbazole (**H₃L₂₇**) (26.3 mg, 0.05 mmol) and 69% concentrated nitric acid (20 μL) in the mixture of DMA (2 ml) and H₂O (0.5 ml) at 348 K for 4 days gave rise to lavender prism crystals of **TCZ-Dy** (22.1 mg, Yield: 54.5%). Anal. Calcd (%) for C₃₇H₃₃N₂O₁₀Dy: C 53.66, H 4.01, N 3.38. Found: C 54.36, H 4.06, N 3.38.

Synthesis of [Ho(L₂₇)(DMA)(H₂O)·3H₂O]_n (TCZ-Ho)

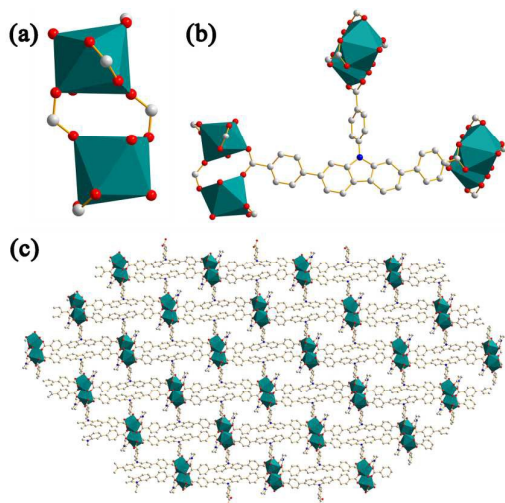


Fig.1 (a) Secondary building units (SBUs) of **TCZ-M** ($M = \text{Nd, Sm, Eu, Gd, Tb, Dy, Ho}$); (b) The coordination environment of deprotonated L_{27} ligand molecule; (c) View of the 3D frameworks in **TCZ-M** ($M = \text{Nd, Sm, Eu, Gd, Tb, Dy, Ho}$).

Solvothermal reaction of $\text{Ho}(\text{NO}_3)_3 \cdot 6\text{H}_2\text{O}$ (22.8 mg, 0.05 mmol), 2,7-bis(4-benzoic acid)-N-(4-benzoic acid) carbazole (H_3L_{27}) (26.3 mg, 0.05 mmol) and 69% concentrated nitric acid (30 μL) in the mixture of DMA (2 ml) and H_2O (0.5 ml) at 348 K for 4 days gave rise to lavender prism crystals of **TCZ-Ho** (21.4 mg, Yield: 52.7%). Anal. Calcd (%) for $\text{C}_{37}\text{H}_{35}\text{N}_2\text{O}_{11}\text{Ho}$: C 52.37, H 4.16, N 3.30. Found: C 52.38, H 4.14, N 3.31.

Single-Crystal Structure Determination.

The X-ray single-crystal structure analyses for the **TCZ-M** ($M = \text{Nd, Sm, Eu, Gd, Tb, Dy, Ho}$) were collected on a Rigaku Saturn 724HG CCD diffractometer (Mo $K\alpha$ radiation $\lambda = 0.71073\text{\AA}$ graphite-monochromator) at 293(2) K. All of the structure were solved by direct methods and refined by full matrix least-squares of F^2 using the SHELXL-2018/1 program.¹⁴ Hydrogen atoms were added in idealized positions. The SQUEEZE routine of the PLATON software suite was used in removing highly disordered solvent molecules.¹⁵ The final formulas were calculated according to the Squeeze results combined with the results from elemental analyses and thermogravimetric

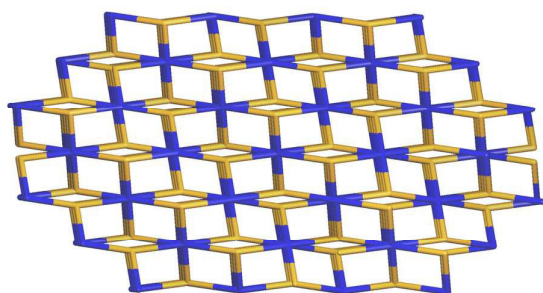


Fig. 2 Topological representation of the 3, 6-connected network in **TCZ-M** ($M = \text{Nd, Sm, Eu, Gd, Tb, Dy, Ho}$).

analysis (TGA).¹⁶ Crystal data for **TCZ-M** ($M = \text{Nd, Sm, Eu, Gd, Tb, Dy, Ho}$) are presented in **Table 1** and **Table 2**. Selected bond lengths and angles of **TCZ-M** ($M = \text{Nd, Sm, Eu, Gd, Tb, Dy, Ho}$) are listed in **Table S1** of Supporting Information.

Photophysical measurements

The solid-state luminescence emission/excitation spectra and solid-state luminescence lifetimes were recorded on an Edinburgh Instruments FLS980 fluorescence spectrophotometer. The quantum yields of the solid-state samples were determined by an absolute method using an integrating sphere on an Edinburgh Instruments FLS920 spectrometer. The lifetimes of the solid-state samples were acquired on an Edinburgh Analytical FLS920 instrument with a Picoseconds Laser Diode.

Results and discussion

Crystal structure of **TCZ-M** ($M = \text{Nd, Sm, Eu, Gd, Tb, Dy, Ho}$)

Structural analysis according to single crystal X-ray diffraction indicates **TCZ-M** ($M = \text{Nd, Sm, Eu, Gd, Tb, Dy, Ho}$) are isomorphous, crystallize in the monoclinic $P2_1/c$ space group. As shown in **Fig.1**, **TCZ-M** ($M = \text{Nd, Sm, Eu, Gd, Tb, Dy, Ho}$) exhibit 3D frameworks and the asymmetric unit includes a fully deprotonated L_{27} ligand, a respective lanthanide metal cation, a coordinated DMA molecule, a coordinated H_2O molecule and two or three free H_2O molecules. Each lanthanide metal cation is eight coordinated by four O atoms from two carboxyl groups of L_{27} ligands, an O atom from a DMA molecule, an O atom from a H_2O molecule and two O atoms from two carboxyl groups which are the bridge between two lanthanide metal cations.

Topologically, the L_{27} ligand could be regarded as 3-connected node and two lanthanide metal cations bridged by two carboxyl groups of L_{27} ligands could be simplified as a 6-connected node. As shown in **Fig.2**, the structure of **TCZ-M** ($M = \text{Nd, Sm, Eu, Gd, Tb, Dy, Ho}$) can be described as a rtl rutile 3, 6-connected network with a Schläfli symbol of $\{4 \cdot 6^2\}_2\{4^2 \cdot 6^{10} \cdot 8^3\}$.¹⁷

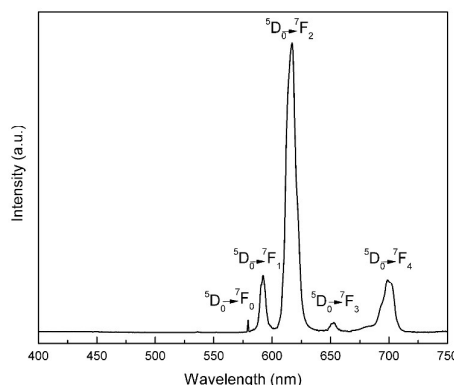


Fig. 3 Solid-state emission spectra of **TCZ-Eu**.

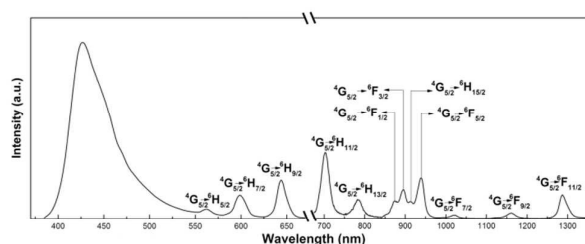


Fig. 4 Solid-state emission spectra of TCZ-Sm.

X-ray powder diffraction and thermal analysis

Powder X-ray diffraction (PXRD) for the bulk samples of **TCZ-M** (**M** = Nd, Sm, Eu, Gd, Tb, Dy, Ho) were carried out at room temperature. The experimental PXRD patterns also prove that **TCZ-M** (**M** = Nd, Sm, Eu, Gd, Tb, Dy, Ho) are isomorphous structures and all of them correspond well with the simulated from the data of single crystal X-ray diffraction and are shown in **Fig. S2** and **Fig. S3**. To estimate the thermal stability, thermogravimetric analysis (TGA) experiments were performed on polycrystalline samples of **TCZ-M** (**M** = Nd, Sm, Eu, Gd, Tb, Dy, Ho) under a N_2 atmosphere with a heating rate of $10\text{ }^\circ\text{C}\cdot\text{min}^{-1}$ in the range of $30 - 800\text{ }^\circ\text{C}$. From room temperature to $170\text{ }^\circ\text{C}$, a weight loss of $3 - 5\%$ is ascribed to the loss of the free solvent molecules between the crystals. From 175 to $275\text{ }^\circ\text{C}$, free solvent molecules and coordinated DMA molecules were removed generally with a weight loss of $19 - 22\%$. The framework collapses and decomposes after $540\text{ }^\circ\text{C}$. (**Fig. S4**)

Photoluminescence properties

The photoluminescence properties of **TCZ-M** (**M** = Nd, Sm, Eu, Gd, Tb, Dy, Ho) and **H₃L₂₇** ligand were investigated under room temperature. The photophysical data are summarized in **Table 3**. The free solid-state **H₃L₂₇** ligand shows a blue fluorescent emission band at 459 nm under 375 nm wavelength excitation with decay lifetime $\tau_{\text{H}_3\text{L}_{27}} = 3.78\text{ ns}$, which is probably due to $\pi^* \rightarrow \pi$ transitions.¹⁸ Under excitation at 399 nm , the solid-state emission spectrum of **TCZ-Eu** was observed with sharp and well-resolved emission peaks (**Fig. 3**). **TCZ-Eu** displays emission bands at $580, 592, 617, 652, 699\text{ nm}$ in the visible region with decay lifetimes about $470\text{ }\mu\text{s}$, coming from the ${}^5\text{D}_0 \rightarrow {}^7\text{F}_J$ ($J = 0,$

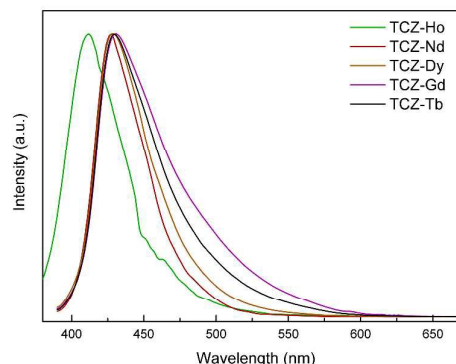


Fig. 5 Solid-state emission spectra of TCZ-M (**M** = Nd, Gd, Tb, Dy, Ho).

$1, 2, 3, 4$) transitions of Eu^{3+} ions. The most intense emission peak at 618 nm is due to the electric dipole induced ${}^5\text{D}_0 \rightarrow {}^7\text{F}_2$ transition, which is highly sensitive to the coordination environment of Eu^{3+} ions. With lower site symmetry of Eu^{3+} ions, the intensity of the emission peak at 618 nm increases obviously. The second intense emission at 594 nm corresponds to the magnetic dipole induced ${}^5\text{D}_0 \rightarrow {}^7\text{F}_1$ transition, which is fairly insensitive to the environment of the Eu^{3+} ions.¹⁹

The Sm^{3+} ion in **TCZ-Sm** has rich spectroscopic properties as a result of multiple electronic transitions originating from the ${}^4\text{G}_{5/2}$ energy level to ${}^6\text{H}_J$ ($J = 5/2, 7/2, 9/2, 11/2, 13/2, 15/2$) and ${}^6\text{F}_J$ ($J = 1/2, 3/2, 5/2, 7/2, 9/2, 11/2$). Both visible and near-infrared (NIR) luminescence could be produced by the multiple electronic transitions. So far, Sm^{3+} -based emitting compounds are rather limited and even less are concerned about their near-infrared emissions. Upon excitation at 370 nm at room temperature, the solid sample of **TCZ-Sm** displays multiple emission peaks at 427 (ligand), 562 (${}^6\text{H}_{5/2}$), 598 (${}^6\text{H}_{7/2}$), 644 (${}^6\text{H}_{9/2}$), 704 (${}^6\text{H}_{11/2}$), 786 (${}^6\text{H}_{13/2}$), 872 (${}^6\text{F}_{1/2}$), 896 (${}^6\text{F}_{3/2}$), 914 (${}^6\text{H}_{13/2}$), 940 (${}^6\text{F}_{5/2}$), 1020 (${}^6\text{F}_{7/2}$), 1162 (${}^6\text{F}_{9/2}$), 1287 (${}^6\text{F}_{11/2}$) nm (**Fig. 4**). The nature of these emissions can be confirmed by the measurement of their decay. The broad band centered at 427 nm is attributable to the emission of the **L₂₇** ligand with a decay lifetime 2.22 ns , which is probably due to $\pi^* \rightarrow n$ or $\pi^* \rightarrow \pi$ transitions. The remaining five narrow peaks ($562, 598, 644, 699, 808\text{ nm}$) have decay lifetimes approximately $4.0\text{ }\mu\text{s}$, which are correlated with the transitions from ${}^4\text{G}_{5/2}$ to ${}^6\text{H}_{5/2}, {}^6\text{H}_{7/2}, {}^6\text{H}_{9/2}, {}^6\text{H}_{11/2}, {}^6\text{H}_{13/2}$, respectively.²⁰

Table 3 Photophysical Parameters of **H₃L₂₇** and compounds **TCZ-M** (**M** = Nd, Sm, Eu, Gd, Tb, Dy, Ho).

	H₃L₂₇	TCZ-Nd	TCZ-Sm	TCZ-Eu	TCZ-Gd	TCZ-Tb	TCZ-Dy	TCZ-Ho
$\lambda_{\text{em}}(\text{nm})$	459	426	427, 562, 598, 644, 704, 786, 872, 896, 914, 940, 1020, 1162, 1287	580, 592, 617, 652, 699	430	429	429	413
τ (ns)	3.78	1.63	2.22 and 4×10^3	4.7×10^5	1.15	1.27	1.10	0.83
Φ (%)	14.26	2.11	0.92 (in visible light range)	15.46	7.86	6.63	6.25	< 0.5

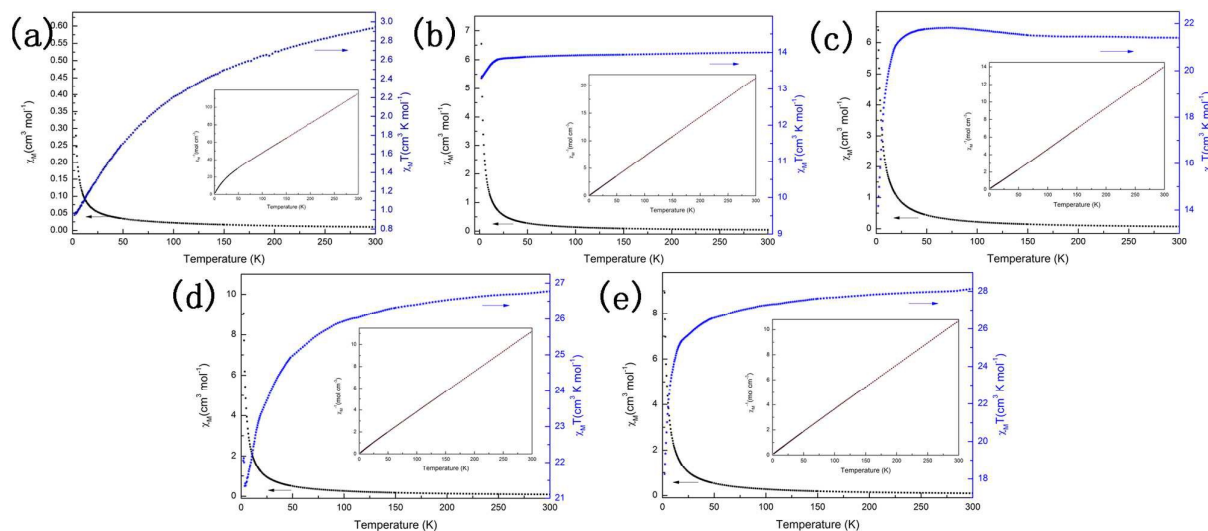


Fig. 6 Plots of χ_M (black), $\chi_M T$ and χ_M^{-1} vs. T for **TCZ-Nd** (a), **TCZ-Gd** (b), **TCZ-Tb** (c), **TCZ-Dy** (d), **TCZ-Ho** (e).

As shown in Fig. 5, the solid-state emission spectra of **TCZ-M** ($M = \text{Nd, Gd, Tb, Dy}$) display intense emission bands centered at 426, 430, 429, 429 nm respectively under excitation at 370 nm. The blue shifts of **TCZ-M** ($M = \text{Nd, Gd, Tb, Dy}$) are tentatively assigned strong electrostatic interaction between the L_{27} ligands and metal ions by donation of the lone pair electrons of O atoms to the empty orbitals of the metal ions.^{13,18a,18d,21} The crystals of **TCZ-Ho** exhibit the blue emission with an emission maximum at 413 nm and the blue shift may due to the absorption of the Ho^{3+} ions in **TCZ-Ho**. (Fig. 5) The emission decay lifetimes of **TCZ-M** ($M = \text{Nd, Gd, Tb, Dy, Ho}$) were found to be $\tau_{\text{TCZ-Nd}} = 1.626$ ns, $\tau_{\text{TCZ-Gd}} = 1.147$ ns, $\tau_{\text{TCZ-Tb}} = 1.274$ ns, $\tau_{\text{TCZ-Dy}} = 1.103$ ns and $\tau_{\text{TCZ-Ho}} = 0.829$ ns.

Magnetic properties

The magnetic properties were measured using a crystalline sample, whose phase purity was confirmed by powder X-ray diffraction. The temperature-dependent magnetic susceptibility of **TCZ-M** ($M = \text{Nd, Sm, Eu, Gd, Tb, Dy, Ho}$) was investigated in the range of 2 – 300 K at a direct current field of 1.0 kOe.

Magnetic studies that this series of Ln-MOFs shows different magnetic properties. The results are illustrated in Fig. 6 as plots of $\chi_M T$ and χ_M versus T , where χ_M is the molar magnetic susceptibility.

The magnetic properties of lanthanide (III) ions are obviously different from those of 3d ions. The 4f orbitals are shielded by the fully occupied 5s and 5p orbitals and the unfilled magnetic shell of electrons (the 4f shell) imbedded in the interior of the ion. The 4fⁿ electrons are almost not involved in the bonds between the lanthanide (III) ion and its nearest neighbors. This makes the energy states of the 4fⁿ configurations approximate to the energy states of the free ions in a first approximation. The influence of the environment

in Ln-MOFs is much less pronounced than in the 3d ions in most of MOFs.²²

As shown in Fig. 6a, the $\chi_M T$ value at room temperature for **TCZ-Nd** is $2.96 \text{ cm}^3 \cdot \text{K} \cdot \text{mol}^{-1}$ and the value is close to the expected values of $3.28 \text{ cm}^3 \cdot \text{K} \cdot \text{mol}^{-1}$ for two uncoupled Nd^{3+} ions ($g_{\text{Nd}} = 8/11$, $S = 9/2$). The temperature dependence of the reciprocal molar susceptibility above 50 K follows the Curie-Weiss law with $C = 3.18 \text{ cm}^3 \cdot \text{K} \cdot \text{mol}^{-1}$, $\theta = -48.03$ K. The relatively big negative Weiss constant indicates dominating antiferromagnetic interactions between Nd^{3+} ions.

The $\chi_M T$ value of **TCZ-Gd** at 300 K is $14.00 \text{ cm}^3 \cdot \text{K} \cdot \text{mol}^{-1}$, which is slightly lower than the expected value ($15.59 \text{ cm}^3 \cdot \text{K} \cdot \text{mol}^{-1}$) of two isolated spin-only Gd^{3+} ions ($g_{\text{Gd}} = 1.99$, $S = 7/2$). The $\chi_M T$ value of **TCZ-Gd** keeps steadily from room temperature to 18 K with decreasing temperature. Upon cooling, the $\chi_M T$ value of **TCZ-Gd** rapidly decreased to a value of $13.30 \text{ cm}^3 \cdot \text{K} \cdot \text{mol}^{-1}$. The magnetic behavior in the temperature range of 2-300 K follows the Curie-Weiss Law with $C = 14.00 \text{ cm}^3 \cdot \text{K} \cdot \text{mol}^{-1}$ and Weiss constant $\theta = -0.398$ K

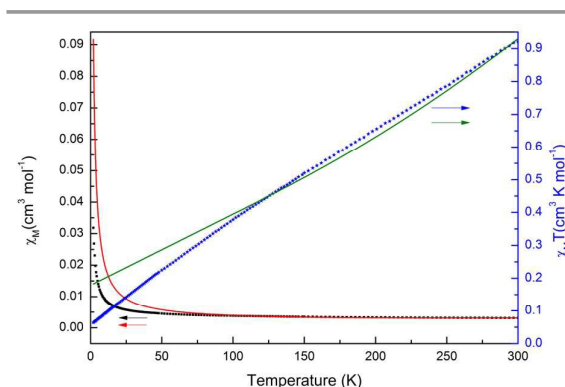


Fig. 7 Plots of χ_M (black) and $\chi_M T$ (blue) vs. T for **TCZ-Sm**; the solid line corresponds to the best fit of χ_M (red) and $\chi_M T$ (green) through eqn (1).

which indicates that there is weak antiferromagnetic coupling between the adjacent Gd^{3+} ions. Theoretically, Gd^{3+} ions with $4f^7$ configuration are very stable in terms of the surrounding environment. Its ground state is the $^8S_{7/2}$, there is no spin-orbit coupling since $L = 0$, the first excited state is 30000 cm^{-1} above the ground state, the crystal field has no noticeable effect on its magnetic properties. (Fig. 6b)²³

For **TCZ-Tb**, the room temperature $\chi_M T$ value is $21.39 \text{ cm}^3 \cdot \text{K} \cdot \text{mol}^{-1}$, which is close to the theoretical value of $23.6 \text{ cm}^3 \cdot \text{K} \cdot \text{mol}^{-1}$ for two Tb^{3+} ions ($g_{\text{Tb}} = 3/2$, $S = 6$). Upon cooling, the value increases gradually to reach a maximum of $21.81 \text{ cm}^3 \cdot \text{K} \cdot \text{mol}^{-1}$ at 64 K. And then decreases to $14.17 \text{ cm}^3 \cdot \text{K} \cdot \text{mol}^{-1}$ at 2 K. The magnetic behavior in the temperature range of 2–300 K follows the Curie–Weiss Law with $C = 21.45 \text{ cm}^3 \cdot \text{K} \cdot \text{mol}^{-1}$ and Weiss constant $\theta = 0.077 \text{ K}$. And there is weak ferromagnetic coupling between the Tb^{3+} ions at higher temperature. (Fig. 6c)

As shown in Fig. 6d, the $\chi_M T$ value at room temperature for **TCZ-Dy** is $28.33 \text{ cm}^3 \cdot \text{K} \cdot \text{mol}^{-1}$ and the value is in agreement with the expected values of $26.77 \text{ cm}^3 \cdot \text{K} \cdot \text{mol}^{-1}$ for two uncoupled Dy^{3+} ions ($g_{\text{Dy}} = 4/3$, $S = 15/2$). The χ_M of TCZ-Dy obeys the Curie–Weiss law over the whole temperature range and resulted in $C = 26.96 \text{ cm}^3 \cdot \text{K} \cdot \text{mol}^{-1}$, $\theta = -3.17 \text{ K}$. The negative θ value of TCZ-Dy indicates the dominance of antiferromagnetic interactions between the Dy^{3+} ions.

The $\chi_M T$ value of **TCZ-Ho** at 300 K is $28.14 \text{ cm}^3 \cdot \text{K} \cdot \text{mol}^{-1}$, which is very close to the expected value ($28.12 \text{ cm}^3 \cdot \text{K} \cdot \text{mol}^{-1}$) of two isolated spin-only Ho^{3+} ions ($g_{\text{Ho}} = 5/4$, $S = 8$). Moreover, the curves of χ_M^{-1} vs T in 2–300 K obey the Curie–Weiss law ($C = 28.19 \text{ cm}^3 \cdot \text{K} \cdot \text{mol}^{-1}$, $\theta = -2.58 \text{ K}$), indicating the occurrence of weak antiferromagnetic coupling between adjacent Ho^{3+} ions. (Fig. 6e)

The ground term (6H) for Sm^{3+} ions is close in energy to the first excited state and it can be thermally populated at room temperature and above, this causes the deviation of the magnetic susceptibility plot from the Curie law. Since λ is small enough for the first excited state to be thermally populated (around 200 cm^{-1}), the magnetic susceptibility follows the numerical expression given in eqn (1)²³

$$\chi_M = \frac{N\beta^2 A}{3kTx B} \quad (1)$$

With $A = (2.143x + 7.347) + (42.92x + 1.641)e^{-\frac{7x}{2}} + (283.7x - 0.6571)e^{-8x} + (620.6x - 1.94)e^{-\frac{27x}{2}} + (1122x - 2.835)e^{-20x} + (1813x - 3.556)e^{-55x/2}$; $B = 3 + 4e^{-7x/2} + 5e^{-8x} + 6e^{-27x/2} + 7e^{-20x} + 8e^{-55x/2}$; $x = \lambda/kT$.

And N stands for Avogadro's number; β stands for Bohr magneton, k stands for Boltzmann constant, T stands for temperature.

As shown in Fig. 7, the best fit value for the spin-orbit coupling parameter is $\lambda = 196 \text{ cm}^{-1}$. Values around 200 cm^{-1} are considered as expected and the magnetic susceptibility plot reproduced the theoretical values till 100 K. Below 100 K the experimental magnetic susceptibility values lie below the theoretical ones, which suggest some weak antiferromagnetic couplings amongst the Sm^{3+} ions.^{23b}

Similar to Sm^{3+} , the ground term (7F) of Eu^{3+} is split into six 7FJ levels by the spin-orbit coupling, λ , with J ranging from 0 to 6. The value of λ is small enough for the first excited state to be thermally populated (about 300 cm^{-1}). It also causes the deviation of the magnetic susceptibility plot from the Curie law. The magnetic susceptibility of Eu^{3+} in **TCZ-Eu** follows the numerical expression given in eqn (2):¹⁹

$$\chi_M = \frac{N\beta^2 C}{3kTx D} \quad (2)$$

With $C = 24 + \left(\frac{27x}{2} - \frac{3}{2}\right)e^{-x} + \left(\frac{135x}{2} - \frac{5}{2}\right)e^{-3x} + \left(189x - \frac{7}{2}\right)e^{-6x} + \left(405x - \frac{9}{2}\right)e^{-10x} + \left(\frac{1485x}{2} - \frac{11}{2}\right)e^{-15x} + \left(\frac{2457x}{2} - 13/2\right)e^{-21x}$; $D = 1 + 3e^{-x} + 5e^{-3x} + 7e^{-6x} + 9e^{-10x} + 11e^{-15x} + 13e^{-21x}$; $x = \lambda/kT$.

Best fit of the magnetic susceptibility data to eqn (2) in the temperature range 130 – 300 K gives $\lambda = 358 \text{ cm}^{-1}$. Value around 300 cm^{-1} are considered in the expected range and the magnetic susceptibility plot reproduces the theoretical values till 130 K. (Fig. 8) The deviation observed below 130 K can be due to weak ferromagnetic interactions between the Eu^{3+} ions.^{19b}

Conclusions

In summary, we have successfully prepared seven new Ln-MOFs, **TCZ-M** ($M = \text{Nd}, \text{Sm}, \text{Eu}, \text{Gd}, \text{Tb}, \text{Dy}, \text{Ho}$), with 2,7-bis(4-benzoic acid)-N-(4-benzoic acid) carbazole. All of the seven Ln-MOFs are isomorphous and the structure could be described as a rtl rutile 3, 6-connected network with a Schläfli symbol of $\{4 \cdot 6^2\}_2\{4^2 \cdot 6^{10} \cdot 8^3\}$. The strong photoluminescence of **TCZ-Eu** indicates it may be good potential candidates for red luminescent materials. For **TCZ-Sm**, it shows sensitized luminescence both in visible and near-infrared region. And other Ln-MOFs, **TCZ-M** ($M = \text{Nd}, \text{Gd}, \text{Tb}, \text{Dy}, \text{Ho}$), also display strong emissions in the visible region, which are similar to the

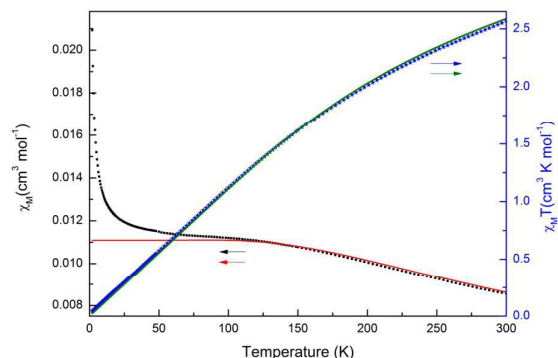


Fig. 8 Plots of χ_M (black) and $\chi_M T$ (blue) vs. T for TCZ-Eu; the solid line corresponds to the best fit of χ_M (red) and $\chi_M T$ (green) through eqn (2).

emission of the ligands. And the seven isomorphous MOFs with different luminescent properties indicates that they may be good potential candidates for luminescent materials by doping the lanthanide metal ions. The magnetic properties of **TCZ-M** (M = Nd, Sm, Eu, Gd, Tb, Dy, Ho) are very different, though the magnetic centers are mediated through the same carboxylate bridge. The Tb³⁺ ions in **TCZ-Tb** exhibit weak ferromagnetic coupling between the adjacent Tb³⁺, while weak antiferromagnetic coupling between adjacent ions occurs in **TCZ-M** (M = Nd, Gd, Dy, Ho). The Eu³⁺ in **TCZ-Eu** and the Sm³⁺ in **TCZ-Sm** is governed by the spin-orbit coupling and the deviations from the theoretical expression being as well due to the splitting of the ground term at low temperatures together with some magnetic interaction.

Acknowledgements

The authors gratefully acknowledge financial support from the National Natural Science Foundation of China (21233009 and 21203194), the 973 program (2014CB845603), the Strategic Priority Research Program of the Chinese Academy of Sciences , Grant No. XDB20000000.

References

- (a) X. Sun, Y. Wang and Y. Lei, *Chem. Soc. Rev.*, **2015**, 44, 8019; (b) M. G. Campbell, S. F. Liu, T. M. Swager and M. Dincă, *J. Am. Chem. Soc.*, **2015**, 137, 13780; (c) Z. Hu, B. J. Deibert and J. Li, *Chem. Soc. Rev.*, **2014**, 43, 5815; (d) L.D. Tran, J. Ma, A. G. Wong-Foy and A. J. Matzger, *Chem. Eur. J.*, **2016**, 22, 5509; (e) P. Q. Liao, X. W. Chen, S. Y. Liu, X. Y. Li, Y. T. Xu, M. Tang, Z. Rui, H. Ji, J. P. Zhang and X. M. Chen, *Chem. Sci.*, **2016**, 7, 6528; (f) H. Xu, X. F. Liu, C. S. Cao, B. Zhao, P. Cheng and L. N. He, *Adv. Sci.*, **2016**, 3, 1600048; (g) J. B. DeCoste and G. W. Peterson, *Chem. Rev.*, **2014**, 114, 5695; (h) Y. Guo, X. Feng, T. Han, S. Wang, Z. Lin, Y. Dong and B. Wang, *J. Am. Chem. Soc.*, **2014**, 136, 15485; (i) Y. M. Li, H. J. Lun, C. Y. Xiao, Y. Q. Xu, L. Wu, J. H. Yang, J. Y. Niu and S. C. Xiang, *Chem. Commun.*, **2014**, 50, 8558; (j) R.-B. Lin, S. Xiang, H. Xing, W. Zhou, B. Chen, *Coord. Chem. Rev.*, **2017**, 41, <https://doi.org/10.1016/j.ccr.2017.09.027>; (k) L. Wang, Y. Ye, Z. Li, Q. Lin, J. Ouyang, L. Liu, Z. Zhang and S. Xiang, *Cryst. Growth Des.*, **2017**, 17, 2081.
- (a) D. J. Tranchemontagne, J. L. Mendoza-Cortes, M. O'Keeffe and O. M. Yaghi, *Chem. Soc. Rev.*, **2009**, 38, 1257; (b) Z. G. Gu, C. Zhan, J. Zhang and X. Bu, *Chem. Soc. Rev.*, **2016**, 45, 3122; (c) D. H. Chen, T. L. Sheng, X. Q. Zhu, L. L., Y. H. Wen, S. M. Hu, R. B. Fu and X. T. Wu, *Z. Anorg. Allg. Chem.*, **2017**, 643, 999; (d) Y. Ye, S. Xiong, X. Wu, L. Zhang, Z. Li, L. Wang, X. Ma, Q. H. Chen, Z. Zhang and S. Xiang, *Inorg. Chem.*, **2016**, 55, 292; (d) Y. Ye, W. Guo, L. Wang, Z. Li, Z. Song, J. Chen, Z. Zhang, S. Xiang and B. Chen, *J. Am. Chem. Soc.*, **2017**, 139, 15604; (e) Y. Wen, T. Sheng, X. Zhu, C. Zhuo, S. Su, H. Li, S. Hu, Q. L. Zhu and X. Wu, *Adv. Mater.*, **2017**, 29, 1700778.
- (a) D. Yang, Y. Tian, W. Xu, X. Cao, S. Zheng, Q. Ju, W. Huang and Z. Fang, *Inorg. Chem.*, **2017**, 56, 2345; (b) H. Ma, L. Wang, J. Chen, X. Zhang, L. Wang, N. Xu, G. Yang and P. Cheng, *Dalton Trans.*, **2017**, 46, 3526; (c) M. N. Akhtar, Y. C. Chen, M. A. Aldamen and M. L. Tong, *Dalton Trans.*, **2017**, 46, 116; (d) Y. Han, P. Yan, J. Sun, G. An, X. Yao, Y. Li and G. Li, *Dalton Trans.*, **2017**, 46, 4642.
- (a) L. Chen, H. Zhang, M. Pan, Z. W. Wei, H. P. Wang, Y. N. Fan and C. Y. Su, *Chem. Asian J.*, **2016**, 11, 1765; (b) J. M. Stanley, B. J. Holliday, *Coord. Chem. Rev.*, **2012**, 256, 1520; (c) J. An, C. M. Shade, D. A. Chengelis-Czegán, S. Petoud, N. L. Rosi, *J. Am. Chem. Soc.*, **2011**, 133, 1220; (d) D. J. Lewis, P. B. Glover, M. C. Solomons, Z. Pikramenou, *J. Am. Chem. Soc.*, **2011**, 133, 1033; (e) J. Zhao, Y. N. Wang, W. W. Dong, Y. P. Wu, D. S. Li and Q. C. Zhang, *Inorg. Chem.*, **2016**, 55, 3265.
- (a) C. Rincke, H. Schmidt and W. Voigt, *Z. Anorg. Allg. Chem.*, **2017**, 643, 437; (b) J. Q. Tao, W. W. Ju, Z. Zhou, L. Y. Jia, N. N. Chen, Y. S. Xue, J. Wang and X. C. Huang, *Z. Anorg. Allg. Chem.*, **2016**, 642, 1466.
- (a) S. Biswas, H. S. Jena, S. Goswami, S. Sanda and S. Konar, *Cryst. Growth Des.*, **2014**, 14, 1287; (b) H. S. Lu, L. Bai, W. W. Xiong, P. Li, J. Ding, G. Zhang, T. Wu, Y. Zhao, J. M. Lee, Y. Yang, B. Geng, Q. Zhang, *Inorg. Chem.*, **2014**, 53, 8529; (c) J. J. Li, T. T. Fan, X. L. Qu, H. L. Han and X. Li, *Dalton Trans.*, **2016**, 45, 2924.
- N. Dannenbauer, P. R. Matthes, T. P. Scheller, J. Nitsch, S. H. Zottnick, M. S. Gernert, A. Steffen, C. Lambert and K. Mueller-Buschbaum, *Inorg. Chem.*, **2016**, 55, 7396.
- (a) W. Morris, W. E. Briley, E. Auyeung, M. D. Cabezas and C. A. Mirkin, *J. Am. Chem. Soc.*, **2014**, 136, 7261; (b) J. Yu, Y. Cui, C. D. Wu, Y. Yang, B. Chen and G. Qian, *J. Am. Chem. Soc.*, **2015**, 137, 4026; (c) P. Falcaro, R. Ricco, C. M. Doherty, K. Liang, A. J. Hill and M. J. Styles, *Chem. Soc. Rev.*, **2014**, 43, 5513.
- H. Ji, X. Li, D. Xu, Y. Zhou, L. Zhang, Z. Zuhra and S. Yang, *Inorg. Chem.*, **2017**, 56, 156.
- (a) M. S. Wang, S. P. Guo, Y. Li, L. Z. Cai, J. P. Zou, G. Xu, W. W. Zhou, F. K. Zheng, G. C. Guo, *J. Am. Chem. Soc.*, **2009**, 131, 13572; (b) D. F. Sava, L. E. Rohwer, M. A. Rodriguez and T. M. Nenoff, *J. Am. Chem. Soc.*, **2012**, 134, 3983.
- (a) L.-Y. Zhang, L.-P. Lu, M.-L. Zhu and S.-S. Feng, *CrystEngComm*, **2017**, 19, 1953; (b) M. N. Akhtar, Y. C. Chen, M. A. Aldamen and M. L. Tong, *Dalton Trans.*, **2017**, 46, 116.
- G. A. Bain and J. F. Berry, *J. Chem. Educ.*, **2008**, 85, 532.
- D. H. Chen, L. Lin, T. Sheng, Y. Wen, S. Hu, R. Fu, C. Zhuo, H. Li and X. Wu, *CrystEngComm*, **2017**, 19, 2632.
- (a) G. M. Sheldrick, SHELXL-97, program for Refining Crystal Structure Refinement, University of Göttingen, Germany, **1997**; (b) G. M. Sheldrick, *Acta Cryst.*, **2015**, 71, 3.
- (a) A. L. Spek, PLATON, Multipurpose crystallographic tool; Utrecht University: Utrecht, The Netherlands, **2001**; (b) A. L. Spek, *Acta Cryst.*, **2009**, 65, 148.
- (a) O. H. bner, A. Glöckner, M. Fichtner and W. Klopfer, *J. Phys. Chem. A*, **2004**, 108, 3019; (c) Y. Wang, C. Tan, Z. Sun, Z. Xue, Q. Zhu, C. Shen, Y. Wen, S. Hu, Y. Wang, T. Sheng and X. Wu, *Chem. Eur. J.*, **2014**, 20, 1341.
- V. A. Blatov, *Struct. Chem.*, **2012**, 23, 955.
- (a) X. T. Zhang, L. M. Fan, W. L. Fan, B. Li, G. Z. Liu, X. Z. Liu and X. Zhao, *CrystEngComm*, **2016**, 18, 6914; (b) X. Y. Wan, F. L. Jiang, L. Chen, J. Pan, K. Zhou, K. Z. Su, J. D. Pang, G. X. Lyu and M. C. Hong, *CrystEngComm*, **2015**, 17, 3829; (c) Y. Gai, F. Jiang, L. Chen, M. Wu, K. Su, J. Pan, X. Wan and M. Hong, *Cryst. Growth Des.*, **2014**, 14, 1010; (d) X. Liu, Z. Xiao, A. Huang, W. Wang, L. Zhang, R. Wang and D. Sun, *New J. Chem.*, **2016**, 40, 5957; (e) L. Lin, D. H. Chen, R. M. Yu, X. L. Chen, W. J. Zhu, D. Liang, J. F. Chang, Q. Zhang and C. Z. Lu, *J. Mater. Chem. C*, **2017**, 5, 4495.
- (a) J. Rong, W. Zhang and J. Bai, *CrystEngComm*, **2016**, 18, 7728; (b) S. I. Klink, L. Grave, D. N. Reinhoudt, F. C. van Veggel, M. H. Werts, F. A. J. Geurts and J. W. Hofstraat, *J. Phys. Chem. A*, **2000**, 104, 5457.
- (a) A. Foucault-Collet, C. M. Shade, I. Nazarenko, S. Petoud and S. V. Eliseeva, *Angew. Chem. Int. Ed.*, **2014**, 53, 2927; (b) L. Sun, Z. Wang, J. Z. Zhang, J. Feng, J. Liu, Y. Zhao and L. Shi, *RSC Adv.*, **2014**, 4, 28481; (c) S. Biju, Y. K. Eom, J.-C. G. Binzli, H. K. Kim, *J. Mater. Chem. C*, **2013**, 1, 6935.

Journal Name

ARTICLE

- 21 H. Y. Liu, H. Wu, J. F. Ma, Y. Y. Liu, B. Liu and J. Yang, *Cryst. Growth Des.*, **2010**, 10, 4795.
- 22 (a) L. Sorace, C. Benelli and D. Gatteschi, *Chem. Soc. Rev.*, **2011**, 40, 3092; (b) A. J. Freeman and R. E. Watson, *Phys. Rev.*, **1962**, 127, 2058.
- 23 (a) O. Kahn, *Molecular Magnetism*, VCH, New York, **1993**; (b) B. Gil-Hernández, J. K. Maclaren, H. A. Höpfe, J. Pasán, J. Sanchiz and C. Janiak, *CrystEngComm*, **2012**, 14, 2635.

Graphical Abstract

Seven isomorphous lanthanide metal-organic frameworks with special luminescence and magnetic properties are synthesized and characterized.

